The role of meridional density differences for a wind-driven overturning circulation

J. Schewe* **and A. Levermann**

Earth System Analysis, Potsdam Institute for Climate Impact Research
Physics Institute, Potsdam University
Potsdam, Germany

Revised version
Submitted to
Climate Dynamics

March 24th, 2009

*correspondence: jacob.schewe@pik-potsdam.de; Potsdam Institute for Climate Impact Research, Telegrafenberg A62, 14473 Potsdam, Germany.

Abstract

Experiments with the coupled climate model CLIM*BER*-3α, which contains an oceanic general circulation model, show deep upwelling in the Southern Ocean to be proportional to the surface wind stress in the latitudinal band of Drake Passage. At the same time, the distribution of the Southern Ocean upwelling onto the oceanic basins is controlled by buoyancy distribution; the inflow into each basin being proportional to the respective meridional density difference. We observe approximately the same constant of proportionality for all basins, and demonstrate that it can be directly related to the flow geometry. For increased wind stress in the Southern Ocean, the overturning increases both in the Atlantic and the Indo-Pacific basin. For strongly reduced wind stress, the circulation enters a regime where Atlantic overturning is maintained through Pacific upwelling, in order to satisfy the transports set by the density differences. Previous results on surface buoyancy and wind stress forcing, obtained with different models, are reproduced within one model in order to distill a consistent picture. We propose that both Southern Ocean upwelling and meridional density differences set up a system of conditions that determine the global meridional overturning circulation.

1 Introduction

The understanding of the driving mechanism* of the Atlantic meridional overturning circulation (AMOC) has evolved along two main theories (*Kuhlbrodt et al.*, 2007). One common view is that the formation of North Atlantic deep water (NADW) is balanced by diapycnal upwelling in the low latitudes of the Atlantic or Indo-Pacific, driven by downward diffusion of heat due to turbulent mixing in the ocean layers above the NADW (*Munk*, 1966; *Munk and Wunsch*, 1998; *Huang*, 1999; *Wunsch and Ferrari*, 2004). Various conceptual models have been designed which contain this type of AMOC driving mechanism (e.g. *Stommel*, 1961; *Zickfeld et al.*, 2004; *Marzeion and Drange*, 2006; *Johnson et al.*, 2007). Especially in zonally averaged models, meridional density (or pressure) differences have often been assumed to be key in setting the overturning rate of the AMOC (*Marotzke et al.*, 1988; *Wright and Stocker*, 1991, 1992; *Hughes and Weaver*, 1994; *Wright et al.*, 1998). Upon the assumption of an idealized density distribution in the Atlantic, *Marotzke* (1997) relates the meridional overturning rate to meridional density gradients in a conceptual model. *Rahmstorf* (1996) showed a linear relation between the meridional density gradients in the Atlantic and the overturning rate in an ocean general circulation model (OGCM) in response to freshwater perturbations.

An alternative theory (*Toggweiler and Samuels* (1993, 1995, 1998)) involves wind-driven deep upwelling in the Southern Ocean (SO) due to the so-called Drake Passage effect: Strong westerlies induce a divergent northward Ekman transport in the latitudes of Drake Passage (DP). Because of the lack of any continental boundaries in these latitudes, the net (i.e., zonally averaged) zonal pressure gradient above the sill of the Passage must be zero. No net geostrophically balanced north-south flow can develop to compensate for the northward surface transport. Therefore, waters from below the sill are drawn up to the surface. The AMOC can be seen as the closing branch of this wind-driven overturning. *Nof* (2003), upon integrating the momentum balance of a water column along a closed contour around the Southern Ocean, came to the conclusion that the Atlantic inflow and outflow is controlled exclusively by Southern Ocean wind stress, and *Levermann et al.* (2007) showed in a coupled climate model that the AMOC can be greatly reduced by a reduction of SO wind stress. The potential of eddy momentum fluxes to possibly compensate part of the wind-driven upwelling is currently subject to discussion (*Hallberg and Gnanadesikan*, 2006; *Naveira Garabato et al.*, 2007).

Gnanadesikan (1999) and *Gnanadesikan et al.* (2007) incorporated these Southern Ocean processes into a model for the global overturning. Herein the meridional density gradient is a fixed parameter, while density changes are represented by the vertical pycnocline depth. However, *Levermann and Griesel* (2004) find that meridional (as opposed to vertical) density changes dominate overturning changes in a coupled climate model. In the meantime, advection and diffusion of temperature and salinity have been incorporated in *Gnanadesikan* (1999)-like models (*Johnson and Marshall*, 2002; *Marzeion and Drange*, 2006). Such an approach is supported by various experiments with an OGCM coupled to a simple moisture balance model described by *Griesel and Morales-Maqueda* (2006), who point out that both Southern Ocean winds and meridional density/pressure gradients play a role in determining the strength of the Atlantic MOC.

*We use the term 'driving mechanism' in the sense of the mechanism providing the input of potential energy required to sustain a deep overturning circulation.

In the following, we attempt to extend and generalize this idea, and give a picture of the global MOC in which both wind-driven Southern Ocean upwelling and meridional density differences combine to set the magnitude and structure of the circulation. To this end, we analyse experiments in a coupled coarse-resolution climate model with both weakened and amplified Southern Ocean wind stress, as well as simulations with anomalous freshwater flux applied to the North Atlantic. The experiments are briefly described in section 2, as well as the model itself, which has a very low background vertical diffusivity ($0.3 \cdot 10^{-4} m^2/s$) and thus operates close to the limit of no diapycnal mixing in the ocean interior. We find in section 3 that the AMOC is, under pre-industrial boundary conditions, almost entirely driven by Southern Ocean winds, but that different regimes are associated with different wind stress conditions. In section 4, we show that, independent of the flow regime, the meridional density difference along the Deep Western Boundary current (DWBC) in each of the basins is a measure for the strength of the respective branch of the global MOC, and that a quasi-universal linear relation exists between the overturning rate and these density differences. We discuss the results in section 5 and conclude that, in our model, both wind-driven Southern Ocean upwelling and meridional density differences combine to set up a coherent system of conditions that determines the magnitude and structure of the global MOC.

2 Models and Experiments

The global coupled climate model CLIM*BER*-3α (*Montoya et al.*, 2005) combines a three-dimensional ocean general circulation model based on the GFDL MOM-3 code with a statistical-dynamical atmosphere model (*Petoukhov et al.*, 2000) and a dynamic and thermodynamic sea-ice model (*Fichefet and Maqueda*, 1997). The oceanic horizontal resolution is $3.75^\circ \times 3.75^\circ$ with 24 variably spaced vertical levels. In order to reduce numerical diffusion a second order moment tracer advection scheme is applied (*Prather*, 1986; *Hofmann and Maqueda*, 2006). Two vertical mixing parameterizations are employed in the model: Mixing enhancement over rough topography with stratification-dependent mixing coefficients, after *Hasumi and Suginohara* (1999) and *Ledwell et al.* (2000), and the KPP boundary layer mixing scheme of *Large et al.* (1994). We apply an eddy transport parameterization following *Gent and McWilliams* (1990), with a thickness diffusivity of $250 m^2/s$. In this study, an improved version of the model is used, comprising a deeper Indonesian throughflow and wind stress prescribed according to the reanalysis of *Trenberth et al.* (1989), and apply a very low background value of vertical diffusivity ($0.3 \cdot 10^{-4} m^2/s$). Thus the mixing induced upwelling in both the Atlantic and Pacific ocean in this model is, for pre-industrial boundary conditions, very small (*Mignot et al.*, 2006).

In the SO, the wind stress field τ_x controls the upwelling of deep water via Ekman divergence: A south-to-north gradient of westerly wind stress in the latitude band of Drake Passage, between $63.75^\circ S$ and $56.25^\circ S$, generates a divergent northward Ekman transport, which cannot be compensated for by any shallow geostrophic return flow, nor from south of the DP, and thus leads to upwelling from depths below the highest topographic ridges in these latitudes (*Toggweiler and Samuels*, 1995, cf. figure 1). For the present study, the zonal oceanic wind stress component τ_x between $71.25^\circ S$ and $30^\circ S$ is modified following $\tau_x(x,y) = \alpha \cdot \tau_x^0(x,y)$, where $\tau_x^0(x,y)$ is the standard wind stress according to *Trenberth et al.* (1989). Experiments were conducted for $\alpha = 0.2$, 0.5, 1.0 and 1.5 , and thus span a range of both reduced and enhanced forcing conditions (figure 1a). In particular, the wind stress at the northern edge of the DP latitude band, which sets the Ekman transport that has to be replaced by deep upwelling, varies from $0.36\, dyn/cm^2$ in the $\alpha = 0.2$ experiment, to $2.70\, dyn/cm^2$ in the $\alpha = 1.5$ experiment. For each experiment, the model was run for at least 7000 years until an equilibrium state was reached.

For comparison, three additional runs were carried out with freshwater flux (FWF) into the North Atlantic (30°–$50^\circ N$, 75°–$7.5^\circ W$) enhanced by $0.35\, Sv$, and with a compensating negative FWF into the North Pacific (30°–$50^\circ N$, $150^\circ E$–$120^\circ W$). In these runs, the observed SO wind stress field was multiplied by $\alpha = 0.5$, 1.0 and 1.5, as described above.

3 Wind-driven Southern Ocean upwelling

We compute Southern Ocean upwelling from the global meridional overturning streamfunction (cf. figure 1b). The depth of the approximate level of no mean motion between the zonally averaged upper northward flow into the Atlantic ocean and the outflow of North Atlantic Deep Water in our model, $780\,m$, serves as reference depth (cf. figure1c). This depth is fairly constant in all our wind stress experiments, as well as in the freshwater flux experiments presented below (*Levermann and Griesel*, 2004). Deep upwelling through the $780m$ depth level in Drake Passage latitudes ($63.75°S$ to $56.25°S$) is directly proportional to the zonally averaged wind stress at $56.25°S$ (figure 2, circles). It equals the Ekman transport at these latitudes (figure 2, dashed line). Thus the slope can be computed analytically via

$$\oint_{56.25°S} \tau_x \cdot (f\rho_0)^{-1} dx = 17.8 \, \frac{Sv}{dyn\, cm^{-2}} \tag{1}$$

A large part of this DP upwelling recirculates within the Southern Ocean north of the DP, forming the so-called Deacon cell (*Döös and Webb*, 1994). When the net upwelling across the Southern Ocean south of $30°S$, which equals the global meridional streamfunction at $30°S$ and $780m$, is considered, the Deacon cell cancels out. Net SO upwelling (figure 2, triangles) is thus only a fraction of the amount of water initially drawn to the surface by Ekman pumping within DP latitudes. Note that we apply an eddy transport parameterization following *Gent and McWilliams* (1990), with a thickness diffusivity of $250m^2/s$. This reduces the effective Deacon cell as it is used in the tracer transport equations, but does not affect the momentum equation. Here we consider solely the effects of the momentum equation. While observations from the Southern Ocean indicate that potential vorticity gradients are weak at the depths of NADW outflow (*Speer et al.*, 2000) and thus the eddy upwelling and downwelling terms might indeed be comparatively small in these depths, other studies suggest that eddy-induced momentum transport could be able to compensate deep wind-driven upwelling to a certain degree (*Hallberg and Gnanadesikan*, 2006; *Naveira Garabato et al.*, 2007). In either case, the qualitative mechanisms depicted in this study would remain valid.

We now relate net SO upwelling to the southward meridional transports out of the different basins. The net SO upwelling can be decomposed by computing the outflow at $30°S$ below $780m$ from the Atlantic (figure 3a, circles) and Indo-Pacific (squares) ocean basins. Both scale linearly with the wind stress. In the standard configuration, all the upwelling in the Southern Ocean is supplied from the Atlantic, thus drawing on the southward branch of the AMOC. The Indo-Pacific basin does not contribute to SO upwelling; instead, there is a small deep inflow of about $1\,Sv$ into the Indo-Pacific basin. Quantitatively, this is not consistent with observational data, which suggest a deep inflow of several Sv into the Indo-Pacific (*Talley et al.*, 2003; *Ganachaud and Wunsch*, 2000, 2003). However, we focus here on the qualitative response of the circulation to wind stress changes, which we believe to be robust within the physics represented in our model.

As wind stress is increased, net Southern Ocean upwelling increases more strongly compared to the Atlantic outflow. The difference is supplied from the Pacific and Indian oceans. For reduced wind stress conditions, on the other hand, there is net inflow into the Indo-Pacific basin, which balances the remaining outflow from the Atlantic. This

Indo-Pacific inflow is divided rather evenly among the Pacific and the Indian basin (figure 3b). All of these curves show a quasi-linear dependence on the SO wind stress for reduced as well as for enhanced forcing. Variable vertical diffusivity in the NADW layers of the SO, as represented by the two parameterizations mentioned in section 2, does not change significantly with SO wind stress (not shown). Any other effect by which mixing in the SO might contribute to deep upwelling would also have to be quasi-linear in order to match with our results.

In summary, in CLIM*BER*-3α the AMOC is, for boundary conditions close to pre-industrial climate, entirely maintained by wind-driven upwelling. Given the small vertical diffusivity applied in the model, low-latitude upwelling in the Atlanic is very small (*Mignot et al.*, 2006). There is some recirculation of NADW in the North Atlantic which occurs mainly along the Western Boundary and could, at least partly, be caused by spurious upwelling due to the poorly resolved Western Boundary layer (*Yang*, 2003). *Griesel and Morales-Maqueda* (2006) dicussed this recirculation and emphasized the importance of clearly distinguishing between the maximum of the Atlantic MOC and the Southern Ocean outflow, the latter being the appropriate measure of the interhemispheric circulation.

The magnitude of the South Atlantic outflow, however, is not solely controlled by SO wind stress. Reducing wind stress induces a shift of the circulation regime towards an AMOC sustained by Indo-Pacific low-latitude upwelling, instead of Southern Ocean upwelling. This implies that the smallness of our background vertical diffusivity must be seen relative to the standard configuration with present-day wind stress, and that for substantially different boundary conditions the same diffusivity parameter can allow a significant amount of mixing-driven upwelling. The shift of the circulation regime, together with the observed linearity of the flow rates with respect to SO wind stress, also raises a question about what properties of the ocean ultimately control the ratio of the overturning rates in the different basins. Meridional density differences as a possible candidate will be discussed in the following section.

4 Volume transport and meridional density differences

In our model, deep meridional volume transport is, in all three basins, mainly confined to the western boundaries (figure 4a, vectors, and 4b). Western Boundary Currents (WBCs; *Munk*, 1950) are a well-known feature of the world ocean. A Deep WBC, with a southward flow rate of the order of $10\,Sv$ and a vertical extent of the order of one to several thousand meters, has been observed in the Atlantic (*Richardson*, 1977; *Hogg*, 1983; *Pickart and Smethie Jr.*, 1993), and similar structures occur in the Pacific (*Whitworth et al.*, 1999).

On the other hand, in our simulations, density (or buoyancy) distribution across the basins changes significantly with varying SO wind stress (figure 5). The Southern Ocean experiences the largest density variations (fig. 5, solid lines) because the wind-driven upwelling of deep, dense water masses and the associated outcropping of isopycnals are directly affected (figure 6): Comparing $\alpha = 0.2$ and $\alpha = 1.5$, corresponding isopycnals have a much larger slope for high wind stress than for low wind stress and, north of about $50°S$, reach deeper. Density is also altered in the Northern Hemisphere (figure 5, dashed lines). The steady state ocean circulation obviously adapts to altered SO wind stress with a global redistribution of buoyancy. However, the strongest response is seen in the SO. Additional simulations with enhanced freshwater flux into the North Atlantic were conducted. This is a standard experimental setup to investigate the robustness and sensitivity of AMOC dynamics (*Manabe and Stouffer*, 1995; *Rahmstorf*, 1996; *Rahmstorf et al.*, 2005). The anomalous freshwater flux reduces deep water formation and, by this means, weakens the Atlantic MOC (figure 7, circles). At the same time, sinking increases in the Indo-Pacific, where a compensating negative freshwater flux is applied (squares). Note that the combined outflow from both basins remains constant to balance Southern Ocean upwelling (triangles). The respective functions for the FWF experiments can thus be obtained by a parallel translation from the experiments without FWF. FWF experiments are denoted by empty symbols in figures 5, 7 and 8.

Based on these observations, we make an attempt to link the meridional volume transport to meridional density differences empirically, and suggest an explanation based on classical boundary layer theory. We compute meridional density differences $\Delta\sigma = \sigma_{north} - \sigma_{south}$ for the Atlantic, Pacific, and Indian ocean, at $1100m$ depth (this choice will be explicated below) between a selected region in the north of each basin and a corresponding region in the Southern Hemisphere (figure 4a). All regions are located along the eastern flanks of the continents, comprising the respective Deep Western Boundary currents (DWBCs). At the same time, the southern regions are chosen to capture the density difference induced by the change of wind stress north of the outcropping area (black bars in figure 6). It turns out that Southern Ocean outflow M_{SO} of all experiments follows a quasi-linear relationship with respect to $\Delta\sigma$ (figure 8).

To understand this, we assume that the meridional volume transport associated with the Southern Ocean outflow is confined to a deep western boundary layer where the y-component of the steady state momentum equation is

$$0 \simeq fu = -\rho_0^{-1}\,\partial_y p + \nabla(\underline{\underline{\nu}}\,\nabla v) \tag{2}$$

i.e., a meridional pressure gradient produces a meridional flow along the boundary, with the Coriolis force balanced by the normal force exerted by topography at the western boundary. Here, ρ_0 is the average density. The horizontal components (denoted by ν_{hor} below) of the eddy viscosity tensor $\underline{\underline{\nu}}$ are usually larger than the vertical ones by several orders of magnitude. In our model, the horizontal viscosity ranges from $0.1 \cdot 10^5\, m^2/s$ at the poles to $3.2 \cdot 10^5\, m^2/s$ at the equator, while vertical viscosity is $10 \cdot 10^{-4}\, m^2/s$ (*Montoya et al.*, 2005). We thus neglect the vertical terms. On the other hand, the divergence of the velocity in y-direction, along the western boundary, can be neglected. Equation (2) can therefore be reduced[†] to

$$\partial_y p \simeq \rho_0\, \nu_{hor}\, \partial_x^2 v \tag{3}$$

Using the hydrostatic equation, we write the l.h.s. of eq. (3) as

$$\partial_y p(z') = g\, \partial_y \int_\eta^{z'} dz\, \rho(z) = g \int_D^{z'} dz\, \partial_y \rho(z) = g\, (z' - D)\, \partial_y \rho(\xi') \tag{4}$$

where z', with $D < z' < D + \delta$, is any depth level within the DWBC; D is the position of the level of no motion, which is also the upper limit of the current; δ is the vertical extent of the DWBC; and η is sea surface elevation (cf. figure 9). In the second step, we have used that all horizontal pressure gradients vanish at the level of no motion. In the third step, we have used the mean value theorem, where ξ', with $D < \xi' < z'$, is the depth at which the meridional density gradient equals the mean value across the integration interval. Averaging of eq. (4) across the DWBC yields

$$\langle \partial_y p \rangle_{DWBC} = g\, \frac{\delta}{2}\, \partial_y \rho(\xi) \tag{5}$$

with $D < \xi < D + \delta$. On the r.h.s. of eq. (3), we express $\partial_x^2 v$ in terms of the lateral extent L_x of the DWBC and its maximum velocity v_{max}, and also average across the DWBC:

$$\langle \partial_x^2 v \rangle_{DWBC} = -F_1\, v_{max} / L_x^2 \tag{6}$$

where the minus sign accounts for the southward direction of the flow, and F_1 is a dimensionless factor that depends on the shape of the two-dimensional velocity profile across the DWBC. The integrated volume transport of the DWBC can also be expressed in terms of v_{max}, L_x and the vertical extent δ:

$$M_{DWBC} = \int_0^{L_x} dx \int_D^{D+\delta} dz\, v(x,z) = F_2\, v_{max}\, L_x\, \delta \tag{7}$$

where F_2 is a factor of integration that again depends on the velocity distribution inside the DWBC.

Combining equations (3), (5), (6) and (7), and assuming a mean meridional density gradient $\langle \partial_y \rho \rangle_y = \Delta\rho / L_y$, where L_y is the meridional distance over which the density difference $\Delta\rho$ occurs, we obtain a relation between the meridional volume transport and

[†]Here, we neglect spatial variation of ν_{hor}. In the model, the latitudinal variation of ν_{hor} is small in low and middle latitudes.

meridional density differences:

$$M_{DWBC} = -\frac{g}{\rho_0\,\nu_{hor}}\,\frac{F_2}{F_1}\,L_x^3\,\delta^2\,\frac{\Delta\rho(\xi)}{L_y} = -\frac{g}{\rho_0\,\nu_{hor}}\,\Phi\,\Gamma\cdot\Delta\rho(\xi) \tag{8}$$

where we identify $\Phi = F_2/F_1$ as a dimensionless form factor relating to the shape of the velocity distribution in the x-z-plane across the DWBC, and $\Gamma = L_x^3\,\delta^2/L_y$ as a form factor relating to the geometry of the current. In principle, Φ, Γ, and also the reference depth ξ, can differ from basin to basin; in particular, L_y is obviously much smaller in the Indian ocean, for example, than in the Atlantic. However, for a choice of $\xi = 1100m$, we find the remarkably consistent relationship shown in figure 8. The individual slopes that one would obtain by connecting only data points belonging to the same basin do indeed differ slightly. On the other hand, the fact that the two points with the largest excursion from the linear approximation (the lowest filled circle and the highest filled square in figure 8) belong to the simulations with, compared to the observed wind stress field, the most unrealistic boundary conditions, supports the possibility that a more or less universal relation exists in a certain interval around the present-day wind-stress configuration.

The slope of the linear relation suggested in figure 8 (dashed line) is $\frac{\Delta M_{SO}}{\Delta(\Delta\sigma)} \approx 44\,\frac{Sv}{kg/m^3}$. For a DWBC velocity distribution following a simple quadratic profile, which we believe to be a reasonable approximation, $\Phi = 1/12$ in eq. (8) (a sine profile would yield the slightly larger value π^{-2})[‡]. In our coarse-resolution model, the western boundary layer is only resolved with one grid point in the x-direction (*Montoya et al.*, 2005, compare figure 4b). We assume $L_x = 350\,km$, which corresponds approximately to the model grid spacing. Further, we use an average horizontal viscosity of $3\cdot10^5\,m^2/s$ for the latitudes under consideration. The observed slope can then be reproduced from eq. (8) for example with a choice of $L_y = 8000\,km$ and $\delta = 2500\,m$, which appears reasonable for the flow geometry in the Atlantic; but also with a choice of $L_y = 3000\,km$ and $\delta = 1500\,m$, which would rather resemble the flow geometry in the Indian ocean (compare figure 4a and b). We emphasize again that these parameters are very poorly constrained both by our model results and observational data. A high-resolution model, for example, is likely to resolve the western boundaries more accurately and therefore yield a different set of parameters, including a smaller value for the lateral extent of the boundary layer of the order of $100km$, as suggested by observations (*Lee et al.*, 1996). We merely wish to demonstrate that the consistent quasi-linear relation between meridional volume transport and meridional density differences found here could, in principle, be explained following the theory outlined above, making more or less reasonable assumptions about the properties of the flow geometry.

[‡]An example for a 2-dimensional quadratic profile would be $v(x,z) = 16\,v_{max}\;x(x-L_x)(z-D)(z-D-\delta)/L_x^2\,\delta^2$. An example for a sine profile would be $v(x,z) = v_{max}\,sin(\pi\,x/L_x)\,sin(\pi\,(z-D)/\delta)$.

5 Discussion and conclusions

We have presented results from experiments with a coupled climate model to investigate the role of Southern Ocean wind stress and buoyancy distribution with respect to the global oceanic circulation. The experiments consist of simulations with Southern Ocean wind stress varying from 0.2 to 1.5 times the observed field, and additional simulations with enhanced freshwater flux into the North Atlantic. For each experiment, the model was run into an equilibrium state. The results must be assessed within the limitations set by the relatively coarse resolution of our model, and its lack of atmospheric variability. Also, as mentioned above, the observed deep inflow into the Indo-Pacific of several Sv is not adequately reproduced by our model for the *Trenberth et al.* (1989) wind stress field. Note however that wind stress reconstructions have some uncertainty. For example, the NCEP-NCAR reanalysis is about 25% weaker in the SO (*Kistler et al.*, 2001). For reduced wind stress, CLIM*BER*-3α does exhibit a significant deep Indo-Pacific inflow (figure 3).

In our experiments, Southern Ocean upwelling is proportional to the SO wind stress. A large part of the upwelled water recirculates within the Southern Ocean, forming the so-called Deacon cell. The remaining net upwelling is drawn out of the ocean basins to the north. The distribution of the upwelling onto the Atlantic, Pacific, and Indian basins is determined by buoyancy differences. For present-day wind stress conditions, all the net SO upwelling is drawn out of the Atlantic, and thus balances the net sinking in the North Atlantic. The meridional flows generated by this dipole of northern sinking and southern upwelling constitute the conveyor belt of the Atlantic MOC. For higher wind stress in the SO, part of the additional upwelling is drawn out of the Pacific and Indian basins. For low wind stress, on the other hand, there is a net inflow into the Pacific and Indian oceans that partly balances the remaining outflow from the Atlantic.

We have shown that the strength - and direction - of the meridional overturning circulation in the different basins is set by meridional density differences. The Southern Ocean outflow rates of all basins obey a linear relation with respect to the meridional density difference along the Western Boundary of the respective basin, with a quasi-universal slope. An explanation was offered on the grounds of classical boundary layer theory, and it was demonstrated that the slope of the linear relation can be reproduced making realistic assumptions about the flow geometry. We conclude that, in our model, both wind-driven Southern Ocean upwelling and meridional density differences combine to set up a coherent system of conditions that determines the magnitude and structure of the global MOC. This concept is illustrated by the response of the model to anomalous freshwater fluxes: The total outflow rate remains unchanged, as it is set by the winds; but the individual outflow rates from the different basins change according to the relative shift in the meridional density differences.

The concept presented here is independent of the mechanism of density transformation, because only density differences along the Western Boundary currents are considered. For example, convection in the North Atlantic is not crucial by itself for the functioning of the MOC, but only in setting the density of the deep water mass. The meridional density differences are altered by changing SO winds through the upwelling of deep, dense water masses; but also by other forcings that may be applied to modulate the MOC, such as anomalous freshwater fluxes in the North Atlantic. With regard to the Indo-Pacific, both directions of circulation, i.e. southern *out*flow and *in*flow, obey the linear relation with

respect to meridional density differences, although the mechanisms at work are certainly different for sinking than for upwelling. Nonetheless, detailed description and explanation of these mechanisms are absolutely necessary for a comprehensive understanding of the circulation, and remain subject to further investigations. In particular, our study suggests that, under substantially altered boundary conditions, diapycnal mixing might play a much larger role than it does in the standard configuration of our model, in spite of a low diapycnal mixing coefficient.

A question remains regarding the role of the recirculation associated with the Deacon cell. It has been argued that the Deacon cell is an artifact of averaging in depth-space, and vanishes in density-space (*Döös and Webb*, 1994), or that, in low-resolution models, it is driven by artificial mixing that allows unrealistically large diapycnal downwelling north of Drake Passage (*Toggweiler and Samuels*, 1995). If we were to assume that the deep downwelling associated with the Deacon cell in our model is completely artificial, this would suggest that SO upwelling is directly linked to the meridional transports set by the density differences, and that changes in one quantity result in corresponding changes in the other. For example, changes in Southern Ocean winds would always alter meridional density differences just to an amount where the resulting circulation compensates the changes in wind-driven SO upwelling.

On the other hand, *Toggweiler and Samuels* (1995) admit that wind-driven deep downwelling north of Drake Passage can occur if North Atlantic sinking is limited, which is the case in the theory drafted here. Thus, if the downwelling branch of the Deacon cell were, at least partly, a realistic feature, then this would add a degree of freedom to the circulation budget: The Deacon cell would act as a sink for the difference between SO upwelling set by winds and the meridional circulation set by density differences.

Acknowledgments

We thank A. Naveira Garabato for a helpful discussion on eddy momentum fluxes. J. S. was funded by the Heinrich Böll Foundation.

References

Döös, K., and D. J. Webb (1994), The Deacon Cell and the other meridional cells of the Southern Ocean, *Journal of Physical Oceanography*, *24*(2), 429–442.

Fichefet, T., and M. A. M. Maqueda (1997), Sensitivity of a global sea ice model to the treatment of ice thermodynamics and dynamics, *Journal of Geophysical Research*, *102*, 12,609–12,646.

Ganachaud, A., and C. Wunsch (2000), Improved estimates of global ocean circulation, heat transport and mixing from hydrographic data, *Nature*, *408*, 453–457.

Ganachaud, A., and C. Wunsch (2003), Large-scale ocean heat and freshwater transports during the World Ocean Circulation Experiment, *Journal of Climate*, *16*, 696–705.

Gent, P. R., and J. C. McWilliams (1990), Isopycnal mixing in Ocean Circulation Models, *Journal of Physical Oceanography*, *20*, 150–155.

Gnanadesikan, A. (1999), A simple predictive model for the structure of the oceanic pycnocline, *Science*, *283*, 2077–2079.

Gnanadesikan, A., A. M. de Boer, and B. K. Mignone (2007), A simple theory of the pycnocline and overturning- revisited, in *Past and Future Changes of the Ocean's Meridional Overturning Circulation*, *Geophysical Monograph Series*, vol. 173, edited by A. Schmittner, J. Chiang, and S. Hemming, pp. 19–32.

Griesel, A., and M. A. Morales-Maqueda (2006), The relation of meridional pressure gradients to North Atlantic Deep Water volume transport in an OGCM, *Climate Dynamics*, *26*, 781–799.

Hallberg, R., and A. Gnanadesikan (2006), The role of eddies in determining the structure and response of the wind-driven Southern Hemisphere overturning: Results from the Modeling Eddies in the Southern Ocean (MESO) project, *Journal of Physical Oceanography*, *36*, 2232–2252.

Hasumi, H., and N. Suginohara (1999), Effects of locally enhanced vertical diffusivity over rough bathymetry on the world ocean circulation., *Journal of Geophysical Research*, *104*, 23,364–23,374.

Hofmann, M., and M. A. M. Maqueda (2006), Performance of a second-order moments advection scheme in an Ocean General Circulation Model, *Journal of Geophysical Research*, *111*, C05,006.

Hogg, N. G. (1983), A note on the deep circulation of the western North Atlantic: Its nature and its causes, *Deep-Sea Research*, *30*, 945–961.

Huang, R. (1999), Mixing and energetics of the oceanic thermohaline circulation, *Journal of Physical Oceanography*, *29*, 727–746.

Hughes, T. M. C., and A. J. Weaver (1994), Multiple equilibria of an asymmetric 2-basin ocean model, *Journal of Physical Oceanography*, *24*, 619–637.

Johnson, H. L., and D. P. Marshall (2002), A theory for the surface atlantic response to thermohaline variability, *Journal of Physical Oceanography*, *32*, 1121–1132.

Johnson, H. L., D. P. Marshall, and D. A. J. Sproson (2007), Reconciling theories of a mechanically driven meridional overturning circulation with thermohaline forcing and multiple equilibria, *Climate Dynamics*, *29*, 821–836.

Kistler, R., et al. (2001), The NCEP/NCAR 50-year reanalysis, *Bull. Amer. Meteor. Soc.*, *82*, 247 – 267.

Kuhlbrodt, T., A. Griesel, M. Montoya, A. Levermann, M. Hofmann, and S. Rahmstorf (2007), On the driving processes of the Atlantic meridional overturning circulation, *Reviews of Geophysics*, *45*, RG2001.

Large, W. G., J. C. McWilliams, and S. C. Doney (1994), Oceanic vertical mixing: A review and a model with a nonlocal boundary layer parameterization, *ROG*, *32*, 363–404.

Ledwell, J. R., E. T. Montgomery, K. L. Polzin, L. C. Schmitt, and J. M. Toole (2000), Evidence for enhanced mixing over rough topography in the abyssal ocean, *Nature*, *403*, 179–182.

Lee, T. N., W. E. Johns, R. J. Zantopp, and E. R. Fillenbaum (1996), Moored observations of Western Boundary Current variability and Thermohaline Circulation at 26.5°N in the subtropical North Atlantic, *Journal of Physical Oceanography*, *26*, 962–983.

Levermann, A., and A. Griesel (2004), Solution of a model for the oceanic pycnocline depth: Scaling of overturning strength and meridional pressure difference, *Geophysical Research Letters*, *31*, L17,302.

Levermann, A., J. Schewe, and M. Montoya (2007), Lack of bipolar see-saw in response to Southern Ocean wind reduction, *Geophysical Research Letters*, *34*(12), L12,711.

Manabe, S., and R. J. Stouffer (1995), Simulation of abrupt climate change induced by freshwater input to the North Atlantic Ocean, *Nature*, *378*, 165–167.

Marotzke, J. (1997), Boundary Mixing and the Dynamics of Three-Dimensional Thermohaline Circulations, *Journal of Physical Oceanography*, *27*, 1713–1728.

Marotzke, J., P. Welander, and J. Willebrand (1988), Instability and multiple steady states in a meridional-plane model of the thermohaline circulation, *Tellus A*, *40*, 162–172.

Marzeion, B., and H. Drange (2006), Diapycnal mixing in a conceptual model of the Atlantic meridional overturning circulation, *Deep-Sea Research II*, *53*(1-2), 226–238.

Mignot, J., A. Levermann, and A. Griesel (2006), A decomposition of the Atlantic meridional overturning circulation into physical components using its sensitivity to vertical diffusivity, *Journal of Physical Oceanography*, *36*, 636–650.

Montoya, M., A. Griesel, A. Levermann, J. Mignot, M. Hofmann, A. Ganopolski, and S. Rahmstorf (2005), The Earth System Model of Intermediate Complexity CLIM*BER*-3α. Part I: description and performance for present day conditions, *Climate Dynamics*, *25*, 237–263.

Munk, W. (1950), On the wind-driven ocean circulation, *J. Meteorol.*, *7*, 80–93.

Munk, W. (1966), Abyssal recipes, *Deep-Sea Research*, *13*, 707–730.

Munk, W., and C. Wunsch (1998), Abyssal recipes II, *Deep-Sea Research I*, *45*, 1977–2010.

Naveira Garabato, A. C., D. P. Stevens, A. J. Watson, and W. Roether (2007), Short-circuiting of the overturning circulation in the Antarctic Circumpolar Current, *Nature*, *447*, 194–197.

Nof, D. (2003), The Southern Ocean's grip on the northward meridional flow, *Prog Oceanogr*, *56*, 223 247.

Petoukhov, V., A. Ganopolski, V. Brovkin, M. Claussen, A. Eliseev, C. Kubatzki, and S. Rahmstorf (2000), CLIMBER-2: a climate system model of intermediate complexity. Part I: model description and performance for present climate, *Climate Dynamics*, *16*, 1–17.

Pickart, R. S., and W. M. Smethie Jr. (1993), How does the deep western boundary current cross the Gulf Stream?, *Journal of Physical Oceanography*, *23*, 2602–2616.

Prather, M. J. (1986), Numerical advection by conservation of second-order moments, *Journal of Geophysical Research*, *91*, 6671–6681.

Rahmstorf, S. (1996), On the freshwater forcing and transport of the Atlantic thermohaline circulation, *Climate Dynamics*, *12*, 799–811.

Rahmstorf, S., et al. (2005), Thermohaline circulation hysteresis: a model intercomparison, *Geophysical Research Letters*, *32*, L23,605.

Richardson, P. L. (1977), On the crossover between the Gulf Stream and the western boundary undercurrent, *Deep-Sea Research*, *24*, 139–159.

Speer, K., S. R. Rintoul, and B. Sloyan (2000), The diabatic Deacon Cell, *Journal of Physical Oceanography*, *30*, 3212–3222.

Stommel, H. (1961), Thermohaline convection with two stable regimes of flow, *Tellus*, *13*, 224–230.

Talley, L. D., J. L. Reid, and P. E. Robbins (2003), Data-based meridional overturning streamfunctions for the global ocean, *Journal of Climate*, *16*, 3213–3226.

Toggweiler, J. R., and B. Samuels (1993), Is the magnitude of the deep outflow from the Atlantic ocean actually governed by southern hemisphere winds ?, in *The Global Carbon Cycle*, edited by M. Heimann, NATO ASI Ser., Ser. I, Springer-Verlag.

Toggweiler, J. R., and B. Samuels (1995), Effect of Drake Passage on the global thermohaline circulation, *Deep-Sea Research*, *42*, 477–500.

Toggweiler, J. R., and B. Samuels (1998), On the ocean's large-scale circulation near the limit of no vertical mixing, *Journal of Physical Oceanography*, *28*, 18321852.

Trenberth, K., J. Olson, and W. Large (1989), A global ocean wind stress climatology based on ECMWF analyses, *Tech. Rep. NCAR/TN-338+STR*, National Center for Atmospheric Research, Boulder, Colorado, USA.

Whitworth, T., B. A. Warren, W. D. Nowlin Jr., S. B. Rutz, R. D. Pillsbury, and M. I. Moore (1999), On the deep western-boundary current in the Southwest Pacific Basin, *Progress in Oceanography*, *43*, 1–54.

Wright, D. G., and T. F. Stocker (1991), A zonally averaged ocean model for the thermohaline circulation. Part I: Model development and flow dynamics., *Journal of Physical Oceanography*, *21*, 1713–1724.

Wright, D. G., and T. F. Stocker (1992), Sensitivities of a zonally averaged global ocean circulation model., *Journal of Geophysical Research*, *97*, 12,707–12,730.

Wright, D. G., T. F. Stocker, and D. Mercer (1998), Closures used in zonally averaged ocean models, *Journal of Physical Oceanography*, *28*, 791–804.

Wunsch, C., and R. Ferrari (2004), Vertical mixing, energy and the general circulation of the oceans, *Annu Rev Fluid Mech*, *36*, 281 314.

Yang, J. (2003), On the importance of resolving the western boundary layer in wind-driven ocean general circulation models, *Ocean Modelling*, *5*, 357379.

Zickfeld, K., T. Slawig, and S. Rahmstorf (2004), A low-order model for the response of the Atlantic thermohaline circulation to climate change, *Ocean Dynamics*, *54*, 8–26.

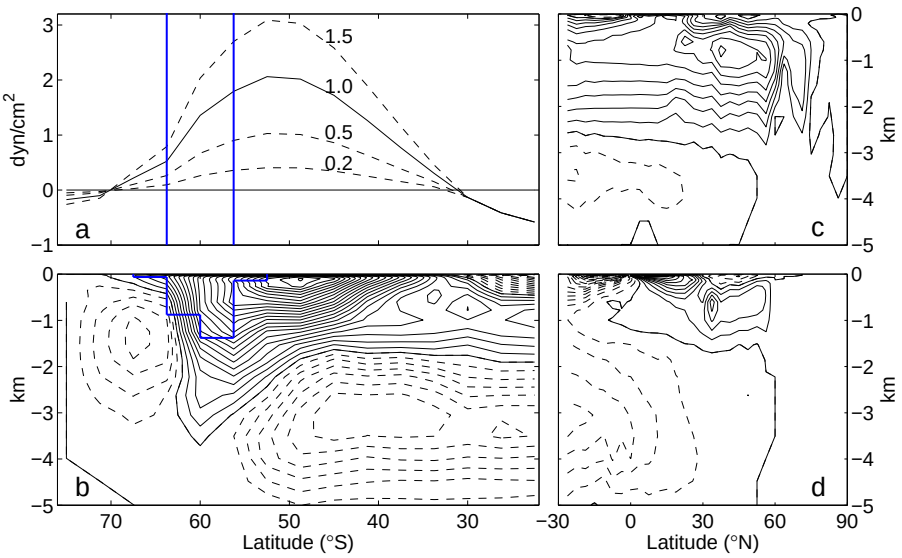

Figure 1: **a)** Zonally averaged, annual mean zonal surface wind stress in Southern Ocean latitudes for the experiments with varying winds. **b)** Global meridional overturning streamfunction in corresponding latitudes, for wind stress forcing according to observations. Spacing between contours is $2\,Sv$, solid (dashed) contours mean clockwise (anticlockwise) circulation. This streamfunction gives only the bulk volume flux, not accounting for tracer advection associated with the parameterization of subgrid-scale eddy motions. The location of the Drake Passage gap in the model (i.e. points with no topographic grid cells at any longitude) is indicated in blue. **c), d)** Meridional overturning streamfunctions for the Atlantic (c) and Indopacific (d) basins, as in b). Note the different x-axis scaling.

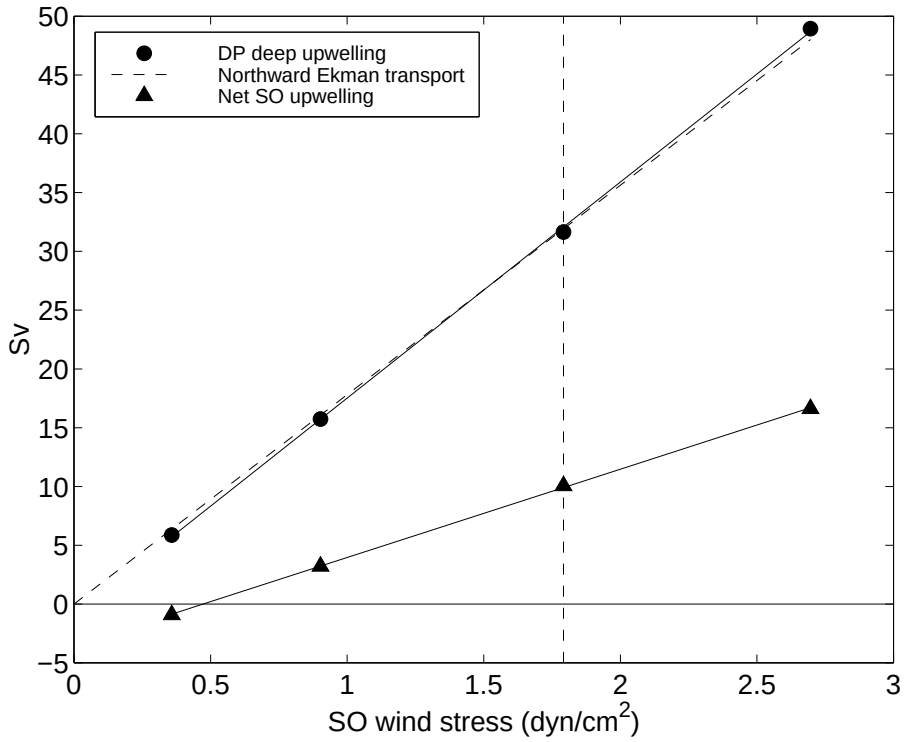

Figure 2: Deep upwelling in Drake Passage latitudes ($63.75°S$ to $56.25°S$; circles) matches the northward Ekman transport out of the DP latitude band, as calculated from $\oint \tau_x \cdot (f\rho_0)^{-1} dx$ (dashed line). Triangles give the net upwelling in the Southern Ocean, i.e. south of $30°S$, where the transport associated with the Deacon cell cancels. Solid lines are linear interpolations. The standard configuration, with present-day wind stress conditions, is indicated by the vertical dashed line

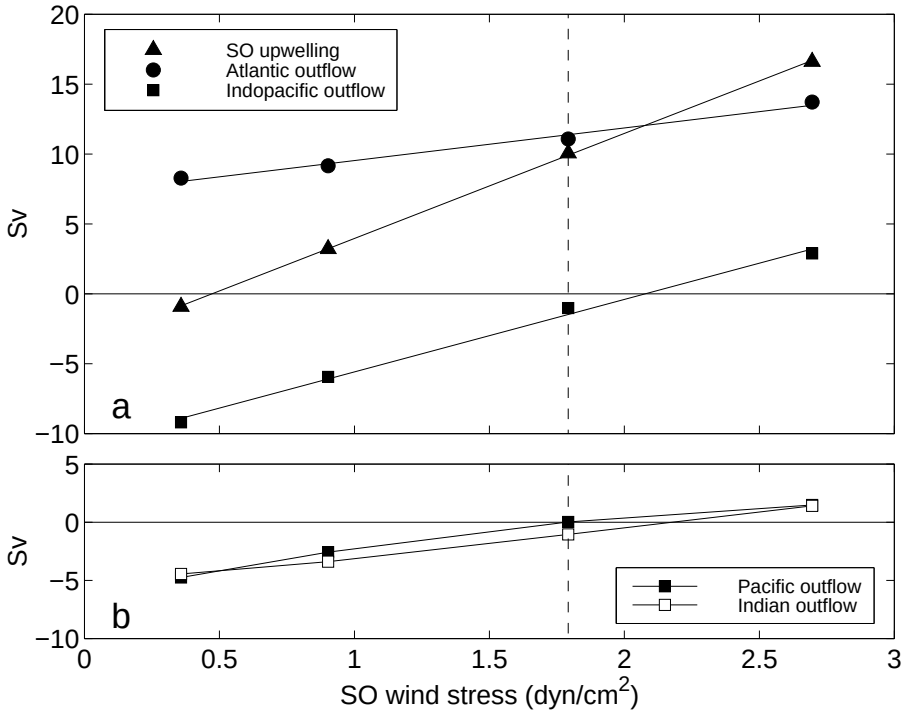

Figure 3: a) The net upwelling south of $30°S$ (triangles, as in figure 2) is a linear function of Southern Ocean wind stress. In the standard configuration (indicated by the vertical dashed line), all of this upwelling is drawn out of the Atlantic (circles). For high wind stress, the Indo-Pacific basin (squares) supplies additional outflow into the SO. For low winds, on the other hand, there is a net upwelling in the Indo-Pacific, which is balanced by comparatively high outflow from the Atlantic. Solid lines are linear interpolations. **b)** Breakdown of the Indo-Pacific outflow rate into individual contributions from the Pacific (filled) and Indian (open squares) oceans, computed from vertical velocities

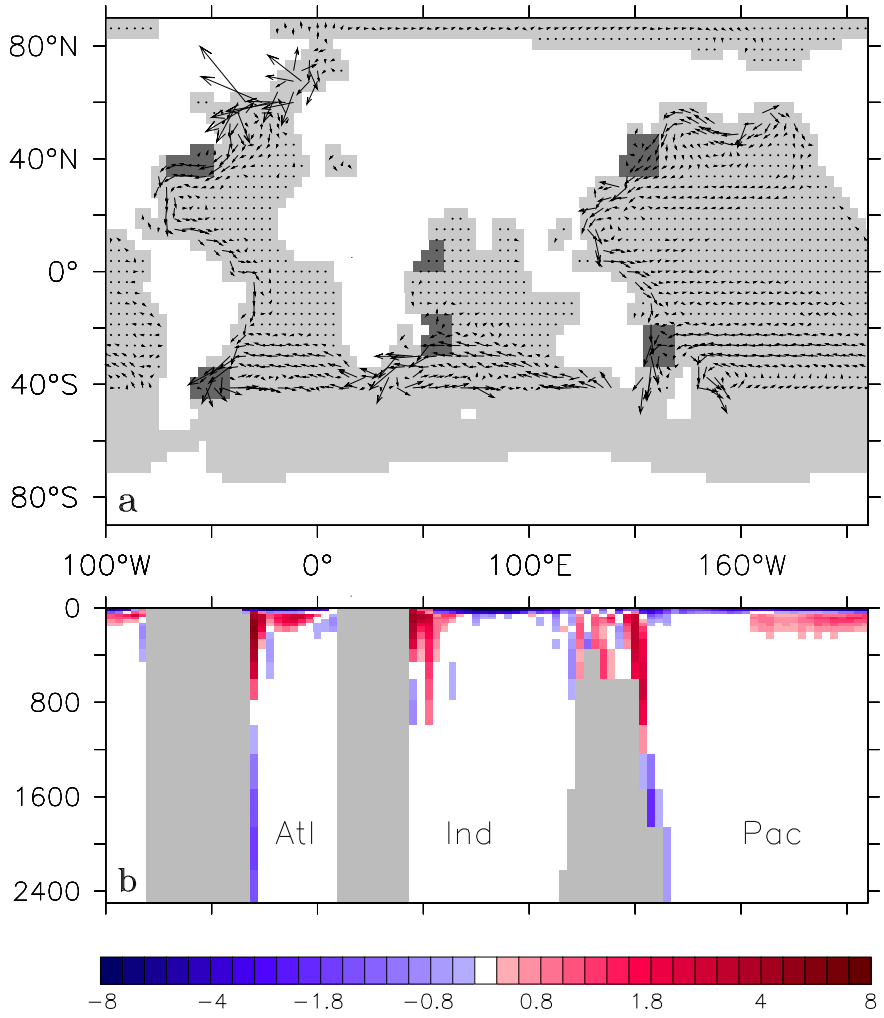

Figure 4: **a)** Ocean regions used to compute meridional density differences. Densities are taken at $1100m$ depth, i.e. within the lower branches of the MOC. The regions are chosen to match the Deep Western Boundary currents (DWBCs) responsible for the main meridional volume transport. Horizontal velocities of the $\alpha = 1.5$ experiment, averaged between $1000m$ and $2000m$ depth, are overlaid as vectors (velocities south of $30°S$ are omitted for the sake of clarity). **b)** Zonal section of meridional velocity at $10°S$ in the $\alpha = 1.5$ experiment, in cm/s. Principal deep currents flow along the western boundaries of the Atlantic, Indian and Pacific oceans

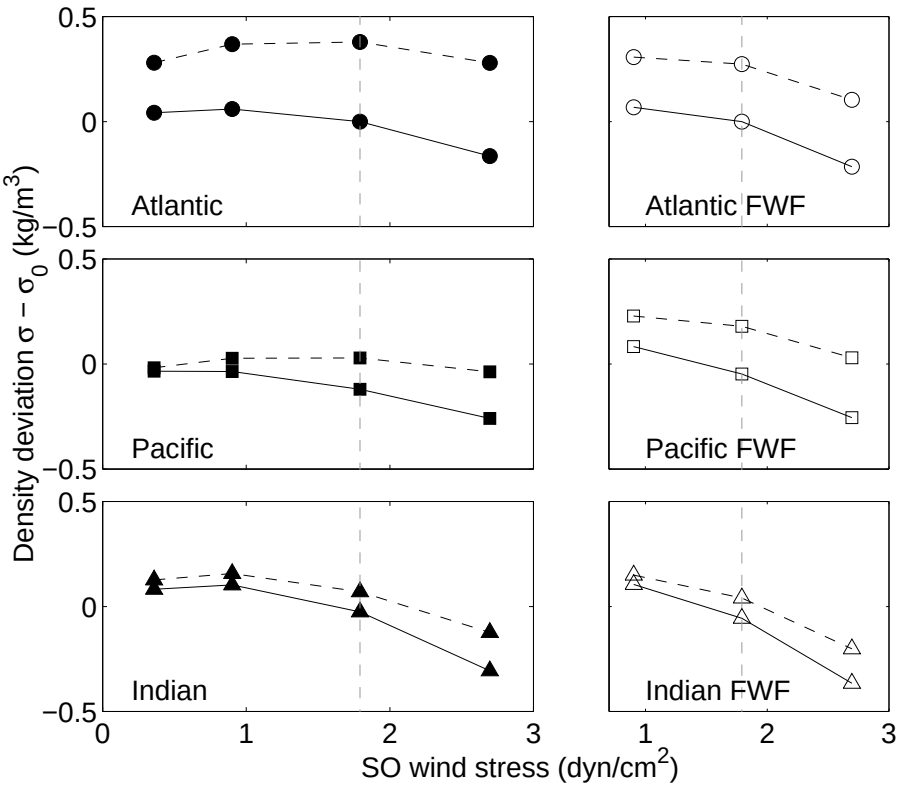

Figure 5: Densities σ_{south} (solid lines) and σ_{north} (dashed lines), as deviation from σ_{south} in the Atlantic at standard wind conditions (σ_0), for the Atlantic (top), Pacific (center) and Indian ocean (bottom). Panels on the right show the FWF experiments. Densities in the south are more strongly affected by changing SO winds. Vertical dashed lines denote the standard wind stress configuration

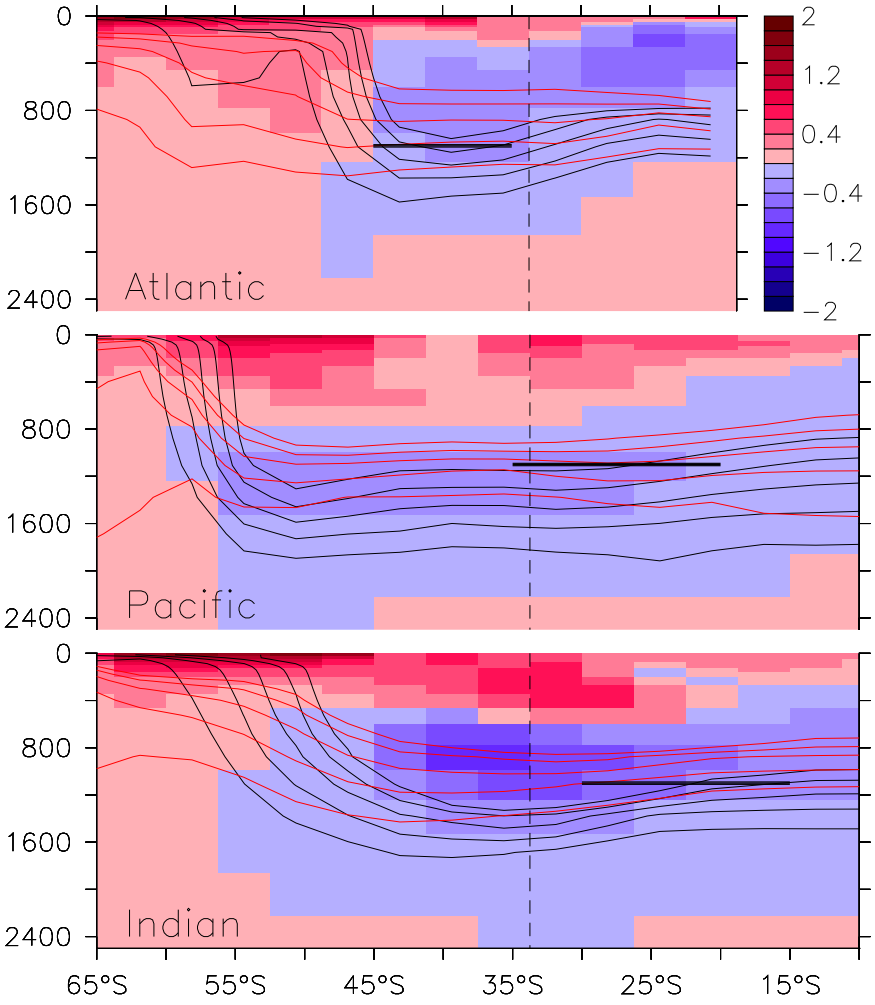

Figure 6: Average density difference between $\alpha = 0.2$ and $\alpha = 1.5$ (colour shading, 1.5 minus 0.2, in kg/m^3) in the southern Atlantic (top), Pacific (center), and Indian ocean (bottom). The black bars indicate the latitudes and depth of the three Southern Hemisphere regions depicted in figure 4a. Five selected, corresponding isopycnals are overlaid each for $\alpha = 1.5$ (black) and $\alpha = 0.2$ (red) to illustrate the change in outcropping and stratification due to changed wind stress. The vertical dashed lines mark the latitude of Cape of Good Hope in the model

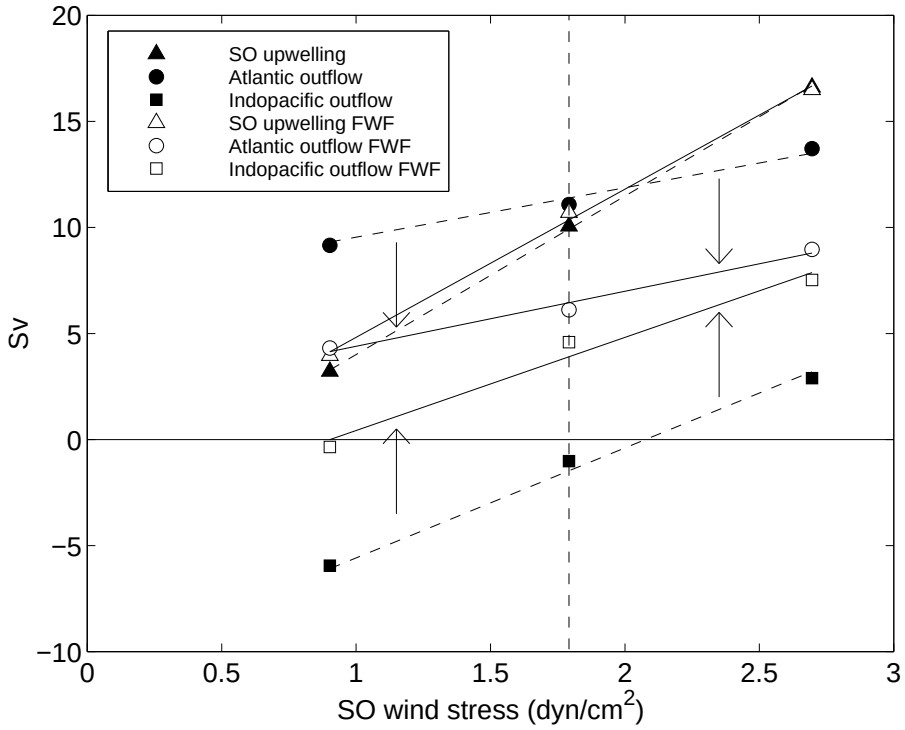

Figure 7: Net Southern Ocean upwelling (triangles) and outflow from the Atlantic (circles) and Indo-Pacific basin (squares), for the experiments shown in figure 3 (filled symbols, dashed lines) and the experiments with anomalous freshwater flux (FWF) applied in the North Atlantic, and compensated for in the North Pacific (empty symbols, solid lines). The standard configuration is indicated by the vertical dashed line. The buoyancy alteration does not change SO upwelling significantly, but leads to a shift in the distribution of the upwelling among the basins, as indicated by the arrows

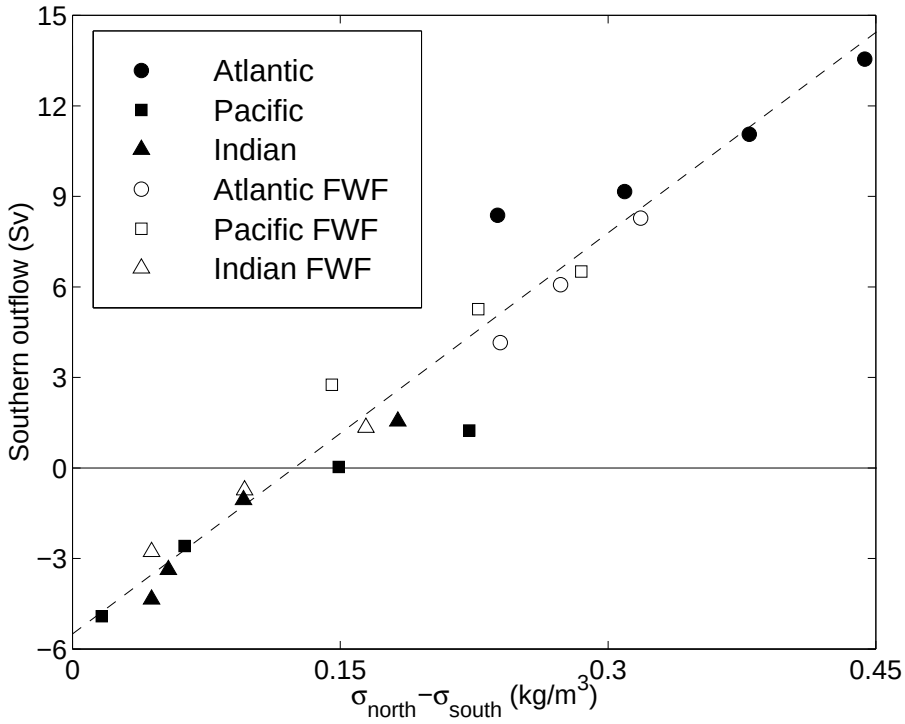

Figure 8: Throughout all experiments, southern outflow from the Atlantic, Indian, and Pacific oceans scales quasi-linearly with the respective meridional density difference at $1100m$ depth. The slope of this relation is approximately the same for all basins. The two points with the largest excursion from the linear approximation (the lowest filled circle and the highest filled square) belong to the simulations with, compared to pre-industrial climate, the most unrealistic boundary conditions.

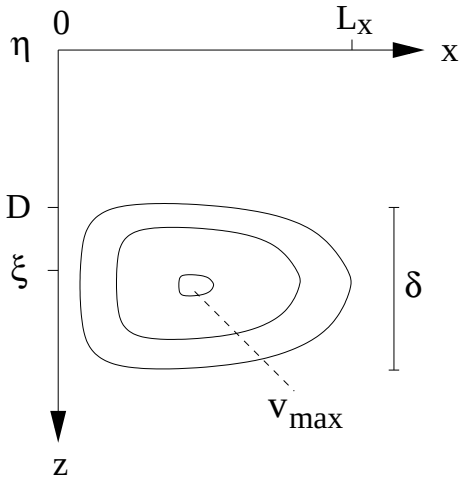

Figure 9: Simplified sketch of an exemplary distribution of southward velocity in a Deep Western Boundary Current, illustrating some of the quantities cited in section 4.